

Molecular BioSystems

Accepted Manuscript



This is an *Accepted Manuscript*, which has been through the Royal Society of Chemistry peer review process and has been accepted for publication.

Accepted Manuscripts are published online shortly after acceptance, before technical editing, formatting and proof reading. Using this free service, authors can make their results available to the community, in citable form, before we publish the edited article. We will replace this *Accepted Manuscript* with the edited and formatted *Advance Article* as soon as it is available.

You can find more information about *Accepted Manuscripts* in the [Information for Authors](#).

Please note that technical editing may introduce minor changes to the text and/or graphics, which may alter content. The journal's standard [Terms & Conditions](#) and the [Ethical guidelines](#) still apply. In no event shall the Royal Society of Chemistry be held responsible for any errors or omissions in this *Accepted Manuscript* or any consequences arising from the use of any information it contains.



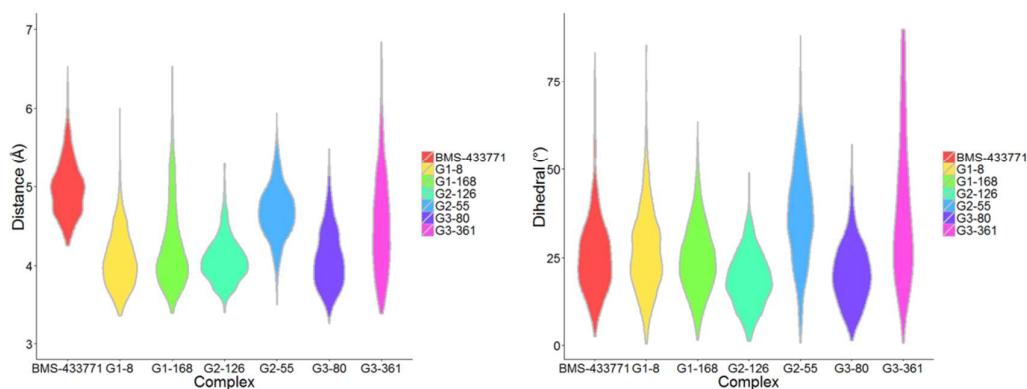
www.rsc.org/molecularbiosystems

Revealing the Binding Mode between Respiratory Syncytial Virus Fusion Receptor and Benzimidazole-based Inhibitors

Dingjue Ji¹, Wei Ye¹, HaiFeng Chen^{*,1,2}

¹State Key Laboratory of Microbial Metabolism, Department of Bioinformatics and Biostatistics, College of Life Sciences and Biotechnology, Shanghai Jiaotong University, 800 Dongchuan Road, Shanghai, 200240, China

²Shanghai Center for Bioinformation Technology, 100 Qinzhou Road, Shanghai, 200235, China



Binding mode between benzimidazole-based inhibitors and RSVF protein was revealed with docking and molecular dynamics simulation.

Revealing the Binding Mode between Respiratory Syncytial Virus Fusion Protein and Benzimidazole-based Inhibitors

Dingjue Ji¹, Wei Ye¹, HaiFeng Chen^{*1,2}

¹State Key Laboratory of Microbial Metabolism, Department of Bioinformatics and Biostatistics, College of Life Sciences and Biotechnology, Shanghai Jiaotong University, 800 Dongchuan Road, Shanghai, 200240, China

²Shanghai Center for Bioinformation Technology, 100 Qinzhou Road, Shanghai, 200235, China

There is not conflict of interest.

*Corresponding authors

Email addresses: haifengchen@sjtu.edu.cn

Tel: 86-21-34204348. Fax: 86-21-34204348.

Abstract Human respiratory syncytial virus (HRSV) is a major respiratory pathogen in newborn infants and young children and also can be a threat to some elderly and high-risk adults with chronic pulmonary disease and the severely immunocompromised. The RSV fusion (RSVF) protein has been an attractive target for vaccine and drug development. Experimental results indicate a series of benzimidazole-based inhibitors which target on RSVF protein to inhibit viral entry of RSV. To reveal the binding mode between these inhibitors and RSVF protein, molecular docking and molecular dynamics simulations were used to investigate the interactions between the inhibitors and the core domain of RSVF protein. MD results suggest that the active molecules have stronger π - π stacking, cation- π , and other interactions than less active inhibitors. The binding free energy between active inhibitor and RSVF protein is also significant lower than that of less active one with MM/GBSA. Then, Comparative Molecular Field Analysis (CoMFA) and Comparative Molecular Similarity Indices Analysis (CoMSIA) methods were used to construct three dimensional quantitative structure-activity (3D-QSAR) models. The cross-validated q^2 values are found as 0.821 and 0.795 for CoMFA and CoMSIA, respectively. And the non-cross-validated r^2 values are 0.973 and 0.961. Ninety-two test set compounds validated these models. The results suggest that these models are robust with good prediction abilities. Furthermore, these models reveal possible methods to improve the bioactivity of inhibitors.

Keywords: respiratory syncytial virus fusion protein; docking; molecular dynamics simulation; 3D-QSAR; inhibitor

Introduction

Human respiratory syncytial virus (HRSV), which was first isolated from chimpanzees with upper respiratory tract illness¹, is a major threat to respiratory health for newborn infants and young children.² Furthermore, HRSV was also found among elderly and high-risk adults with underlying chronic pulmonary disease and the severely immunocompromised, which always suffered upper and lower respiratory disease caused by the virus.³ On average per year in the United States, RSV infection leads to 132,000 to 172,000 hospitalizations among children with 5 years of age, and 100,000 to 126,000 hospitalizations among children with 1 year of age, and 1.5 million outpatient visits among children with 5 years of age.^{4,5}

The fusion of viral membranes with target-cell membranes is essential for the entry of enveloped virus into cells.⁶ Type I viral fusion proteins are synthesized as single-chain precursors and then assembled into trimers.⁶ Three surface glycoproteins of HRSV are named as F, G and SH.⁷ F protein, which consists of disulfide-linked subunits F1 and F2, is an indispensable part of fusion process. In fusion peptide region, a hydrophobic glycine-rich segment is inserted into the membrane of target cell. The C terminus of F1 subunit locates at transmembrane region. Two motifs of 4,3-hydrophobic heptad repeat (HR) with coiled-coil structures are close to fusion and transmembrane regions. After HRSV protein inserts into the fusion region, it can form trimeric hairpin-like structure through a significant conformational change of F protein.⁸ The crystallization of this trimer⁸ has verified its function and provides references for drug design targeting on this protein.

The method of mainstream prevention and therapy to treat RSV is palivizumab⁹. Other promising vaccines such as Medi-534¹⁰ are still on early stage of trials. Therapy with ribavirin has proven beneficial in certain patient populations, particularly critically ill patients on mechanical ventilation and lung transplant recipients.¹¹ Other alternative therapies such as cathelicidin and MDD still remain unknown on underlying danger without further sufficient tests for safety.⁴ New drugs are still needed to be introduced to therapy of RSV.

Actually, kinds of inhibitors have been put into various researches targeting RSV Fusion (RSVF) protein. These inhibitors classed into small peptides and organic molecules. T20⁶ and T118 are potent peptide inhibitors which were designed and synthesized to prevent the fusion of virus.¹² However, considering the cost of production and oral availability and low half-life in circulation, few peptide inhibitors of RSVF protein enter clinical trials.¹³ The other is organic small molecule inhibitors, many of them have passed preclinical study, such as RFI-641¹⁴, VP-14637¹⁵, and BTA-9881¹⁶. These inhibitors of RSVF protein face similar challenges to other lead compounds. For example, RFI-641 has drug resistance to G446R mutant of RSVF and the safety of BTA-9881 remains to be questionable.^{14,17}

Until now, just one complex between RSVF protein and TMC353121¹⁸ was released (PDB: 3KPE). RSVF protein with the clear binding pocket near Y198@A has been discussed and validated in structural biology.^{18,19} It is possible to use computational methods to study compounds targeting on this binding site. In order to improve the efficiency of drug discovery, Comparative Molecular Field Analysis (CoMFA)²⁰ and Comparative Molecular Similarity Indices Analysis (CoMSIA)²¹ have been widely applied to design lead compounds. However, 3D-QSAR model could only illuminate the relationship between substituent and antiviral activity.²² Molecular dynamics simulation (MD) was usually utilized to reveal the interaction mechanism between ligand and receptor. Furthermore, a well-defined X-ray crystal structure (ID: 1G2C) of RSVF protein has been released.⁸ Therefore, we combined 3D-QSAR and MD simulation to better explore the binding mode and construct the prediction model for RSV inhibitors.²³ This 3D-QSAR model can help us to make quantitative prediction of their inhibitory activities before resorting to *in vitro* and *in vivo* experiment.

Methods

Data set

The structure and bioactivity (IC₅₀ μM) of 370 compounds (shown in Supplementary

Table S1) were extracted from the literature.^{24,25,26,27,28,29,30} According to the structure, these compounds were clustered into three groups and representative structures were shown in supplementary Figure 1S. Group 1 and group 2 have common skeleton. For group 3, the skeleton is diverse and different from those of groups 1 and 2. The structures marked with '*' belong to the test set. The others constitute the training set.

Molecular Modeling and Alignment

Three-dimensional structures of inhibitors in Table S1 were built and optimized with SYBYL modeling program (SYBYL-X v1.0 Tripos). The default module of MultiSearch was utilized to search the conformers of each compound. Tripos force field³¹ was applied to perform energy minimization for these structures. Gasteiger-Hückel method was used to calculate partial atomic charges of these structures.

Predictive abilities of CoMFA and CoMSIA models were evaluated by cross-validated q^2 results from Leave-One-Out (LOO) method. It is reported that q^2 has sensitivity to the orientation and alignment of compounds for training set.³² Therefore, the common substructure and the alignment template play key roles in model construction. Molecule BMS-433771 with the typical binding mode (shown in Figure 1), which was as one of synthetic templates and examined *in vivo*³⁰, was chosen as the template of alignment. The SYBYL routine of "Align Database" was used to handle the molecular alignment. These inhibitors from Table S1 were aligned with benzimidazole and/or benzimidazolinone of BMS-433771, respectively.

Figure 1.

Molecular Docking

The crystal structure of RSVF protein core domain (PDB code: 1G2C) was retrieved from the protein data bank for molecular docking. Docking site was referred to the analogous cavity¹⁹ validated by Cianci, C *et al.* Autodock4.0/Vina package³³ was utilized to dock RSVF with the ligands from Table S1. The principle of

AutoDock4.0/Vina has been described elsewhere.^{33,34} During the docking process, the exhaustiveness of global search was set to 20, and the maximum number of conformer was set to 15. Representative docking conformers for BMS-433771 and the structures from supplementary Figure S1B were used as the initial structures for molecular dynamics simulation. 3D-QSAR model was built based on these docking conformers.

CoMFA Models

Comparative Molecular Field Analysis (CoMFA) was derived from the method proposed by Cramer *et al.*²⁰ Firstly, these molecules were aligned within a lattice. This lattice can cover these molecules and be classed into a set of grid size. A sp^3 carbon atom with +1 net charge was employed as a probe to calculate the steric and electrostatic interactions. Secondly, a coulomb potential and a Lennard-Jones potential were used to model electrostatic and Van Der Waals interactions, respectively. Thirdly, the partial least squares (PLS) method³⁵ was applied for regression analysis. Total data set of molecules was randomly divided into training and test sets in the approximate ratio 3:1 (for example, 278 in training set to 92 in the test set).²³

CoMSIA Models

Comparative Molecular Similarity Indices Analysis (CoMSIA) was proposed by Klebe *et al* and used to construct 3D-QSAR model.²¹ Five physicochemical properties of steric, electrostatic, hydrophobic, hydrogen bond donor, and hydrogen bond acceptor fields were applied to describe the interactions between inhibitor and the probe atom. Different from CoMFA, Gaussian-type potential function was used to model these interactions.²³ The potential function in CoMSIA led to much smoother sampling of the fields around the molecules than that in CoMFA. A default value of 0.3 was used as attenuation factor.

Molecular Dynamics Simulation

AMBER12 package³⁶ and ff12SB force field³⁷ were used to perform MD simulations. Initial coordinates of seven representative complexes were extracted from docking conformers. Antechamber module³⁸ was applied to handle the force field of the ligands and AM1-bcc charges were assigned to the ligands. SHAKE algorithm³⁶ was implemented to constrain the bonds involving hydrogen atoms. All systems were solvated in a truncated octahedron box of TIP3P water model³⁹ with a buffer of 10 Å. Partial Mesh Ewald (PME) method⁴⁰ was used to evaluate long range electrostatic interaction. 1000 steps of the steepest descent method were applied to process the energy minimization. The optimized structure was then heated to a finite temperature of 298K followed by a 20ps simulation for equilibration. Then simulations were done at 298K for 20 ns. Eight systems including apo-RSVF, seven bound RSVF with 6 representative compounds and BMS-433771 were selected and simulated. A total of 160ns trajectories was collected for these solvated systems.

Data Analysis

Cpptraj⁴¹ was used to process the trajectories. Hydrophobic interaction, electrostatic interaction, and hydrogen bond assignment were handled with in-house perl script.⁴²⁻⁴³ Hydrophobic interaction is defined as the distance between the center mass of side chain for hydrophobic residue and the hydrophobic center of ligand less than 6.5 Å. Any positively and negatively charged residues are in electrostatic interaction when their mass centers are less than 11 Å. Hydrogen bond is defined when the distance between two polar heavy atoms either with a hydrogen atom was less than 3.5 Å and the angle is larger than 135°. All figures were plotted with ggplot2⁴⁴. Binding free energies were calculated with Molecular Mechanics-Generalized Born Surface Area (MM/GBSA) method⁴⁵ using MMPBSA.py⁴⁶ for the last 5 ns conformers.

Result

Evaluation of binding mode between BMS-433771 and RSVF protein

The previous work proposes a possible binding mode that the benzimidazolone ring of BMS-433771 is located at the C-terminal Phe-488 binding site.¹⁹ The pyridine moiety buries deeply in the groove and sandwiches between chains A and E, near L195@A, L193@E, and V192@E. The benzimidazole ring occupies the C-terminal Phe-483 binding position and is located among Y198@A, K196@E, I199@E, D200@E, and L204@E.¹⁹ In order to evaluate this point, BMS-433771 was docked with RSVF and the docking complex was simulated for 20ns. The root-mean-squared deviation (RMSD) relative to the initial structure was calculated and shown in Figure 2A. The results show that 20 ns simulations are sufficient for the equilibration at room temperature.

Figure 2.

The interaction between BMS-433771 and RSVF is shown in Figure 2B. There are one hydrogen bond and six hydrophobic contacts with population higher than 25%, such as pyridine/L195@A, pyridine/L193@E, pyridine/V192@E, benzimidazole/L204@E, benzimidazole/L199@E, and benzimidazole/L195@A. Hydroxyl group of R₁ forms a hydrogen bond with carboxyl group of D194@A. The average structure of BMS-433771 and RSVF complex is shown in Figure 3. The helical structure of trimer for RSVF is stable except the terminal. The aromatic rings of BMS-433771 are located at the hydrophobic pocket of RSVF. The benzimidazole ring of BMS-433771 also forms π - π stacking with Y198@A or cation- π interaction⁴⁷ with K196@E of RSVF. These results are consistent with the previous work and confirm the reasonability of binding mode.¹⁹

The binding mode of TMC353121 and RSVF protein has been reported and is shown in supplementary Figure S2.¹⁸ Six-membered aromatic ring linked with benzimidazole ring is instead of F483@B and near Y198@A. D200@E and D496@B form two hydrogen bonds with ligand. TMC353121 is almost perpendicular to the

chains of RSVF protein. However, BMS-433771 is parallel with chains A and E of RSVF protein. Therefore, the binding mode of BMS-433771 is different from that of TMC353121 with RSVF.

Figure 3.

Reveal of binding mode for representative inhibitors

Binding mode of BMS-433771 was tested and confirmed by docking and molecular dynamic simulation. Then molecular docking for G1-168, G1-8, G2-55, G2-126, G3-361, and G3-80 with RSVF was performed based on the binding mode of BMS-433771. Six docking complexes were simulated for 20 ns, respectively. The root-mean-squared deviation (RMSD) relative to the initial structure for each complex was calculated and shown in Figure 4A. The results show that 20 ns simulations are sufficient for the equilibration of all systems at 298K. The RMSDs for whole ligand and for skeleton of ligand are also shown in Figures 4B-4C. G1-8, G1-168, and G2-55 have higher fluctuation than other ligands. Furthermore, the RMSD of skeleton suggests that the skeleton of G2-55 presents high fluctuation after 15 ns and G2-55 might escape from the binding pocket of RSVF.

Figure 4.

To illustrate the binding mode, the electrostatic, hydrophobic, and hydrogen bonding interactions for last 5ns were calculated. The population of interaction for six complexes is shown in supplementary Figure S3. In general, the interactions with L195@A and V192@E present in different complexes except G2-55 and those hydrophobic residues lock the aromatic rings of inhibitor within the binding site. This interaction mode is similar to that of BMS-433771.

There are five hydrophobic interactions for G1-8 and G1-168, with population higher than 50%. The differences for G1-8 and G1-168 are just focused on M₁ near V192@E and R₂ near D194@A. The distances between the mass center of six-membered aromatic ring at M₁ and the side chain of V192@E for G1-168 and

G1-8 are shown in Figure 5A. This figure suggests that G1-8 forms potent interaction with V192@E during most of simulation time. However, the pyridine of G1-168 has large fluctuation and only partly forms hydrophobic interaction with V192@E. The distances between the mass center of R₂ and the side chain of D194@A for G1-168 and G1-8 are shown in Figure 5B. R₂ of G1-168 is located at the groove near D194@A (shown in Figure 5C) and it is electrostatically unfavorable for sulfonyl group nearby D194@A. In fact, the decomposition contribution of binding free energy for G1-8 and G1-168 is shown in Figure 5D, respectively. The ΔG of G1-8 is significant lower than that of G1-168.

Figure 5.

For G2-126, there are one electrostatic, one hydrogen bond, and two hydrophobic interactions. Hydrogen bond and hydrophobic interaction of G2-126 are stronger than those of G2-55. The positive charged R₃ group of G2-126 forms stable electrostatic contact with D200@E while the negative charged R₃ group of G2-55 does not. The average structures of G2-126 and G2-55 complexes are shown in Figure 6. The electrostatic interaction between R₃ of G2-55 and K196@E drags M₂ out of the hydrophobic core. The electrostatic repulsion between D200@E and R₃ of G2-55 weakens the interaction between R₃ and chain E. The electrostatic and hydrogen bonding interactions for G3-80 are stronger than those for G3-361. This can explain that the bioactivity of G3-80 is higher than that of G3-361.

Figure 6.

Photo-affinity label indicates that Y198@A is the key marker of binding site¹⁹. To compare with experiment, the π - π interaction between M₂ and benzene ring of Y198@A was calculated to reveal the binding mode. The distance between two benzene rings for face-to-face π - π interaction⁴⁸ is about 3.6~3.8 Å. Considering the distribution of electron atmosphere⁴⁹, the distance between geometrical center of

benzene ring and the dihedral angle for M₂ and Y198@A are used to mark the π - π interaction. The violin plots are shown in Figure 7. Combined with dihedral angle and distance, the π - π interaction of G2-55 and G3-361 is very weak with Y198@A. For G1-8 and G1-168, the distributions of dihedral angle are similar. However, G1-8 was centralized in lower distance than G1-168. In summary, the binding affinity of G1-8 is stronger than that of G1-168. For BMS-433771, G2-126, and G3-80, they are near the origin of coordinate to facilitate the potent π - π interaction.

Figure 7.

Additionally, K196@E as another key marker of binding site, its cation- π interaction⁴⁷ is qualitatively described by the distance between its NZ atom and mass center of aromatic ring for the seven compounds and shown in Figure 8. The position of projection is nearer origin point and the interaction is stronger. This figure indicates that the molecules of BMS-433771, G1-8, G2-126, and G2-80 with high affinity are more centralization near origin point than those of G1-168, G2-55, and G3-361. This could partly explain that the molecules of BMS-433771, G1-8, G2-126, and G2-80 have higher affinity than those of G1-168, G2-55, and G3-361.

Figure 8.

The binding free energy between ligand and RSVF is also calculated and listed in Table 1. Besides mentioned electrostatic effect, G1-168 with polar R₂ exposed in solvent has higher solvation cost, which has negative contribution to the binding affinity. Therefore, the binding free energy for G1-168 is -23.172 kcal/mol and 4.299 kcal/mol higher than that for G1-8. For G2-126 and G2-55, the contribution of VDW for G2-126 is larger than that for G2-55 because M₂ group of G2-55 is exposed in water. G3-80 had more favorable VDW interaction than G3-361. Therefore, the

ΔG_{Total} for G3-80 is lower than that for G3-361. The correlation between the binding free energy and pEC50 for these inhibitors is shown in Figure 9. The correlation coefficient R^2 is 0.858 with p -value of 0.03. This suggests that MD methods are reliable and the results are in quantitative agreement with those of the experimental observation.

Table 1.
Figure 9.

Figure 10 illustrates the superposition of G1-8, G2-126, and G3-80 within RSVF binding pocket. This figure shows three common hydrophobic interactions with residues Leu195@E and Val192@A. The benzimidazole rings of three compounds have similar orientation. In summary, G1-8, G2-126, and G3-80 have similar binding modes with RSVF. Therefore, we could construct common 3D-QSAR models for these RSVF inhibitors.

Figure 10.

3D-QSAR model

Two methods, CoMFA and CoMSIA, were used to construct 3D-QSAR models for 278 training set. The parameters of these models are given in Table 2. The experimental activity and predicted activity are shown in supplementary Table S1.

Table 2.

Evaluation of CoMFA and CoMSIA models

Table 2 lists the statistical parameters of CoMFA and CoMSIA models for inhibitors. The 10-fold cross-validated q^2 of CoMFA model is 0.821 and the non-cross-validated parameter r^2 of the model is 0.973. The correlation between predicted activities (PA) and experimental activities (EA) of training and test sets with

CoMFA model is shown in Figure 11A. The correlation coefficient r^2 between EA and PA of test set is 0.949. In CoMSIA model, the 10-fold cross-validated q^2 is 0.795. The correlation between PA and EA of training and test sets is shown in Figure 11B. The correlation coefficient r^2 between EA and PA of test set is 0.914. The correlation coefficient r^2 suggests that the CoMFA and CoMSIA models are robust and have good prediction ability. For CoMSIA model, there is an outlier and the structure is also shown in Figure 11B. The structure of G2-317 including electron enriched group of cyano is different from other inhibitors of training set. Therefore, this structure might not be well trained.

Figure 11.

Analysis of CoMFA model

The contribution of steric and electrostatic fields of CoMFA model was 0.378 and 0.622, respectively. The contour maps of CoMFA model with structure G3-80 are shown in Figure 12. Blue contour near the R_3 group suggests that positive charged substituent at R_3 position is favorable to activity. This could explain that the activities of compounds G3-80 and G2-126 with positive charged amino group are higher than those with negative charged R_3 of G2-55. Blue and red contours near R_1 and R_2 substituents indicate that suitable charged group is favorable to the bioactivity. This can explain that compound G1-177 with tertiary amino group of R_2 and negatively charged R_1 has high bioactivity. The green-colored regions near R_1 and R_2 groups suggest that bulky substitute is favorable to bioactivity. Actually, the less active molecules of G3-83, G1-176, and G1-180 include with tiny substituent or even no substituent at R_1 group. In summary, the CoMFA model could explain the different activities of training and test sets.

Figure 12.

Analysis of CoMSIA model

The contribution of steric, electrostatic, hydrophobic, hydrogen bond donor and acceptor fields was 0.104, 0.258, 0.187, 0.186, and 0.265, respectively. The contour maps of CoMSIA model with structure G3-80 are shown in supplementary Figure S4. The steric and electrostatic fields of CoMSIA model are similar to those of CoMFA model. Therefore, the other three fields were analyzed. Cyan contour near the R₃ group suggests that hydrogen bond donor substituent is favorable to activity. This could explain that the compounds of G2-126, G3-80, and G3-77 with hydrogen bond donor have high affinity. Magenta-colored regions near R₁ group indicate that hydrogen bond receptor substituent is favorable to the bioactivity. This can explain that the R₁ groups of G1-8, G1-159, and G2-241 with hydrogen bond acceptor have high bioactivity. White-colored regions near M₁ group indicate that hydrophilic substituent is favorable to bioactivity. This can explain that the bioactivity of G3-129 with polar modification of inner ester is higher than that of G3-368 with benzotriazole. Yellow-colored and magenta-colored regions near R₂ group suggest that hydrophobic and hydrogen bond acceptor substituents are favorable to bioactivity. This could explain that the activities have the sequence: G3-188 (3,3-dimethyl) > G3-75 (inner ester), G2-341 (fatty acid) > G2-347 (ammonium). In summary, the CoMSIA model could explain the different activity of training and test sets.

Discussion

Comparison between CoMFA model and MD results

Because the conformations used for 3D-QSAR were obtained from molecular docking, 3D-QSAR contour could be directly compared with the binding mode. The alignment between CoMFA model and the complex G3-80 is shown in supplementary Figure S5. This figure shows that negative charged D200@E is near the positive charged R₃ group of G3-80. The contour plot of electrostatic favorable blue-colored region covers the R₃ group. The red-colored favorable regions cover R₁ substituent and positive charged K196@E. For example, G1-177 and G1-87 with negatively

charged terminal of R₁ form electrostatic interaction with positive charged K196@E. Green and blue contour maps near R₂ group and D194@A suggest that bulky and positive charged groups can be located at the binding pocket. These comparisons suggest that the results of MD simulation are consistent with those of CoMFA model.

Comparison between CoMSIA model and MD results

Because the distribution of contour plot for steric and electrostatic is similar to those of CoMFA, here we just aligned hydrophobic, donor and acceptor fields with G3-80/RSVF complex and shown in Figure 13. D200@E is near R₃ group as a hydrogen bond receptor. This is consistent with the suggestion of cyan contour with hydrogen bond donor favorable region. Furthermore, the R₃ group of G2-126 and G3-80 could form potent hydrogen bond with D200@E in MD simulation. At the same time, K196@E plays a key role as hydrogen bond donor near the magenta contour. For R₂ group, yellow and magenta contours suggest that hydrophobic and hydrogen bond acceptor substituents are favorable to bioactivity. Furthermore, N197@A is a hydrogen bond donor residue and its fatty chain could be located at the groove of RSVF. Additionally, cyan contour indicates that hydrogen bond donor substituent is favorable to bioactivity. And D194@A is located at this place as a hydrogen bond acceptor hydrogen-binding with BMS-433771 from MD simulation. These comparisons suggest that the results of MD simulation are consistent with those of CoMSIA model.

Figure 13.

Based on the comparison between 3D-QSAR models and MD simulation, the detail guide for how to improve the bioactivity of inhibitor is shown in Figure 14. Bulky negative charged or hydrophobic with hydrogen bond acceptor substituent for R₁ is favorable to bioactivity. Bulky positive-charged or hydrophobic with hydrogen bond receptor or donor substituent for R₂ is favorable to bioactivity. For R₃, tiny

positive charged and hydrogen bond donor groups are favorable to the bioactivity. These suggestions can be confirmed with experiment.

Figure 14.

Comparison with previous work of 2D-Classification

Two-dimension molecular descriptors have been used to classify subset for this data set. Mold2⁵⁰ is a potent tool to generate molecular descriptors and used for QSAR or virtual screening. Therefore, Ming Hao *et al*⁵¹ has used Mold2 descriptors to classify RSVF inhibitors. Variable-selection random forest (VS-RF) was used to select key descriptors and do classification for 272 structures. Their distribution of pEC50 values is from 6.5 to 7.5 and their bioactivity is classed into low and active activity. During VS-RF process, 6 Mold2 descriptors (shown in supplementary Table S2⁵¹) were selected in literature. These descriptors were used to compare with the field parameters in 3D-QSAR.

D299, as a topological descriptors, is a molecular branching index calculated from the algebraic formulas derived by Lovasz and Pelikan.⁵² D347 represents molecular topological path index and this index increases with the ring size, ring numbers, and the ramification number.⁵³ D503 and D490 belong to 2D autocorrelation classes, which represent the topological structure of the compounds.⁵¹ These two descriptors are related to the steric variance in different substituents at M₁ or M₂. D513 and D528 belong to topological charge indices. D513 represents the third eigenvalue of the corrected adjacency matrix of a molecule and D528 for the eighth eigenvalue.⁵¹ These descriptors are related with the character of steric and electrostatic. Our 3D-QSAR models also include steric and electrostatic fields. Therefore, these models are in qualitative agreement with the previous work.

Conclusion

CoMFA and CoMSIA methods were used to build 3D-QSAR models on 370 RSVF inhibitors. Correlation coefficient r^2 of test set were 0.949 and 0.914 for these two

models. The result shows that these models process good prediction ability. At the same time, molecular dynamics simulation was used to research the binding mode between some representative inhibitors and RSVF. The result suggests that the most active compounds (G1-8, G2-126, and G3-80) of three groups have stronger interactions than less active compounds (G1-168, G2-55, G3-361) with RSVF. The binding free energy for these high active compounds is significant lower than that for low active compounds, respectively. The binding mode of these representative compounds is similar to that of BMS-433771. Comparison with 3D-QSAR and MD, the results of 3D-QSAR are consistent with those of MD. The comparison also illustrates the way to improve the bioactivity of inhibitors.

Acknowledgements

This work was supported by Center for HPC at Shanghai Jiao Tong University, by grants from the Ministry of Science and Technology of China (2012CB721003), the National High-tech R&D Program of China (863 Program) (2014AA021502), the National Natural Science Foundation of China (J1210047 and 31271403), the Innovation Program of the Shanghai Education Committee (Grants No. 12ZZ023), Medical Engineering Cross Fund of Shanghai Jiao Tong University (YG2013MS68 and YG2014MS47), and data collection came from pRED China Co. Ltd.

Reference:

1. Blount, R. E., Jr.; Morris, J. A.; Savage, R. E., Recovery of cytopathogenic agent from chimpanzees with coryza. *Proc Soc Exp Biol Med* **1956**, *92* (3), 544-9.
2. Hall, C. B.; Weinberg, G. A.; Iwane, M. K.; Blumkin, A. K.; Edwards, K. M.; Staat, M. A.; Aunger, P.; Griffin, M. R.; Poehling, K. A.; Erdman, D.; Grijalva, C. G.; Zhu, Y.; Szilagyi, P., The burden of respiratory syncytial virus infection in young children. *N Engl J Med* **2009**, *360* (6), 588-98.
3. Falsey, A. R.; Hennessey, P. A.; Formica, M. A.; Cox, C.; Walsh, E. E., Respiratory syncytial virus infection in elderly and high-risk adults. *N Engl J Med* **2005**, *352* (17), 1749-59.
4. Turner, T. L.; Kopp, B. T.; Paul, G.; Landgrave, L. C.; Hayes, D., Jr.; Thompson, R., Respiratory syncytial virus: current and emerging treatment options. *Clinicoecon Outcomes Res* **2014**, *6*, 217-25.
5. Protect Against Respiratory Syncytial Virus. Centers for Disease Control and Prevention. *Centers for Disease Control and Prevention* **2014**.
6. Colman, P. M.; Lawrence, M. C., The structural biology of type I viral membrane fusion. *Nature Reviews Molecular Cell Biology* **2003**, *4* (4), 309-319.
7. Collins, P., pp. 1313-1351 of vol. 1, Fields Virology, et al., Eds. Raven Press: 1996.

8. Zhao, X.; Singh, M.; Malashkevich, V. N.; Kim, P. S., Structural characterization of the human respiratory syncytial virus fusion protein core. *Proceedings of the National Academy of Sciences of the United States of America* **2000**, *97* (26), 14172-7.
9. Group, I.-R. S., Palivizumab, a humanized respiratory syncytial virus monoclonal antibody, reduces hospitalization from respiratory syncytial virus infection in high-risk infants. *Pediatrics* **1998**, *102* (3), 531-537.
10. Gomez, M.; Mufson, M. A.; Dubovsky, F.; Knightly, C.; Zeng, W.; Losonsky, G., Phase-I study MEDI-534, of a live, attenuated intranasal vaccine against respiratory syncytial virus and parainfluenza-3 virus in seropositive children. *The Pediatric infectious disease journal* **2009**, *28* (7), 655-658.
11. Hemming, V. G.; Prince, G. A.; Horswood, R. L.; London, W. T.; Murphy, B. R.; Walsh, E. E.; Fischer, G. W.; Weisman, L. E.; Baron, P. A.; Chanock, R. M., Studies of passive immunotherapy for infections of respiratory syncytial virus in the respiratory tract of a primate model. *The Journal of infectious diseases* **1985**, 1083-1087.
12. Lambert, D.; Barney, S.; Lambert, A.; Guthrie, K.; Medinas, R.; Davis, D.; Bucy, T.; Erickson, J.; Merutka, G.; Petteway, S., Peptides from conserved regions of paramyxovirus fusion (F) proteins are potent inhibitors of viral fusion. *Proceedings of the National Academy of Sciences* **1996**, *93* (5), 2186-2191.
13. Sun, Z.; Pan, Y.; Jiang, S.; Lu, L., Respiratory syncytial virus entry inhibitors targeting the F protein. *Viruses* **2013**, *5* (1), 211-25.
14. Razinkov, V.; Gazumyan, A.; Nikitenko, A.; Ellestad, G.; Krishnamurthy, G., RFI-641 inhibits entry of respiratory syncytial virus via interactions with fusion protein. *Chemistry & biology* **2001**, *8* (7), 645-59.
15. McKimm-Breschkin, J., VP-14637 ViroPharma. *Current opinion in investigational drugs* **2000**, *1* (4), 425-7.
16. Bond, S.; Sanford, V. A.; Lambert, J. N.; Lim, C. Y.; Draffan, A. G.; Nearn, R. H.; Mitchell, J. P., Polycyclic Agents for the Treatment of Respiratory Syncytial Virus Infections. Google Patents: 2013.
17. Anderson, K. H.; Draffan, A. G.; Lim, C. Y.; MAYES, P. A.; Mitchell, J. P.; Pitt, G. R. W., Compounds for treating respiratory syncytial virus infections. Google Patents: 2011.
18. Roymans, D.; De Bondt, H. L.; Arnoult, E.; Geluykens, P.; Gevers, T.; Van Ginderen, M.; Verheyen, N.; Kim, H.; Willebrords, R.; Bonfanti, J. F.; Bruinzeel, W.; Cummings, M. D.; van Vlijmen, H.; Andries, K., Binding of a potent small-molecule inhibitor of six-helix bundle formation requires interactions with both heptad-repeats of the RSV fusion protein. *Proceedings of the National Academy of Sciences of the United States of America* **2010**, *107* (1), 308-13.
19. Cianci, C.; Langley, D. R.; Dischino, D. D.; Sun, Y.; Yu, K. L.; Stanley, A.; Roach, J.; Li, Z.; Dalterio, R.; Colonna, R.; Meanwell, N. A.; Krystal, M., Targeting a binding pocket within the trimer-of-hairpins: small-molecule inhibition of viral fusion. *Proceedings of the National Academy of Sciences of the United States of America* **2004**, *101* (42), 15046-51.
20. Cramer, R. D.; Patterson, D. E.; Bunce, J. D., Comparative molecular field analysis (CoMFA). 1. Effect of shape on binding of steroids to carrier proteins. *J Am Chem Soc* **1988**, *110* (18), 5959-67.
21. Klebe, G.; Abraham, U.; Mietzner, T., Molecular similarity indices in a comparative analysis (CoMSIA) of drug molecules to correlate and predict their biological activity. *J Med Chem* **1994**, *37* (24), 4130-46.
22. Sharma, H.; Patil, S.; Sanchez, T. W.; Neamati, N.; Schinazi, R. F.; Buolamwini, J. K., Synthesis, biological evaluation and 3D-QSAR studies of 3-keto salicylic acid chalcones and related amides as

- novel HIV-1 integrase inhibitors. *Bioorg Med Chem* **2011**, *19* (6), 2030-45.
23. Ma, S.; Ye, W.; Ji, D.; Chen, H. F., Insight into the binding mode between HIV-1 integrase and pyrimidone analogue inhibitors with MD simulation and 3D-QSAR. *Med Chem* **2013**, *9* (3), 420-33.
24. Yu, K.-L.; Zhang, Y.; Civiello, R. L.; Kadow, K. F.; Cianci, C.; Krystal, M.; Meanwell, N. A., Fundamental structure–Activity relationships associated with a new structural class of respiratory syncytial virus inhibitor. *Bioorganic & Medicinal Chemistry Letters* **2003**, *13* (13), 2141-2144.
25. Yu, K. L.; Zhang, Y.; Civiello, R. L.; Trehan, A. K.; Pearce, B. C.; Yin, Z.; Combrink, K. D.; Gulgeze, H. B.; Wang, X. A.; Kadow, K. F.; Cianci, C. W.; Krystal, M.; Meanwell, N. A., Respiratory syncytial virus inhibitors. Part 2: Benzimidazol-2-one derivatives. *Bioorg Med Chem Lett* **2004**, *14* (5), 1133-7.
26. Yu, K. L.; Wang, X. A.; Civiello, R. L.; Trehan, A. K.; Pearce, B. C.; Yin, Z.; Combrink, K. D.; Gulgeze, H. B.; Zhang, Y.; Kadow, K. F.; Cianci, C. W.; Clarke, J.; Genovesi, E. V.; Medina, I.; Lamb, L.; Wyde, P. R.; Krystal, M.; Meanwell, N. A., Respiratory syncytial virus fusion inhibitors. Part 3: Water-soluble benzimidazol-2-one derivatives with antiviral activity in vivo. *Bioorg Med Chem Lett* **2006**, *16* (5), 1115-22.
27. Yu, K. L.; Sin, N.; Civiello, R. L.; Wang, X. A.; Combrink, K. D.; Gulgeze, H. B.; Venables, B. L.; Wright, J. J.; Dalterio, R. A.; Zadjura, L.; Marino, A.; Dando, S.; D'Arienzo, C.; Kadow, K. F.; Cianci, C. W.; Li, Z.; Clarke, J.; Genovesi, E. V.; Medina, I.; Lamb, L.; Colonno, R. J.; Yang, Z.; Krystal, M.; Meanwell, N. A., Respiratory syncytial virus fusion inhibitors. Part 4: optimization for oral bioavailability. *Bioorg Med Chem Lett* **2007**, *17* (4), 895-901.
28. Wang, X. A.; Cianci, C. W.; Yu, K. L.; Combrink, K. D.; Thuring, J. W.; Zhang, Y.; Civiello, R. L.; Kadow, K. F.; Roach, J.; Li, Z.; Langley, D. R.; Krystal, M.; Meanwell, N. A., Respiratory syncytial virus fusion inhibitors. Part 5: Optimization of benzimidazole substitution patterns towards derivatives with improved activity. *Bioorg Med Chem Lett* **2007**, *17* (16), 4592-8.
29. Combrink, K. D.; Gulgeze, H. B.; Thuring, J. W.; Yu, K. L.; Civiello, R. L.; Zhang, Y.; Pearce, B. C.; Yin, Z.; Langley, D. R.; Kadow, K. F.; Cianci, C. W.; Li, Z.; Clarke, J.; Genovesi, E. V.; Medina, I.; Lamb, L.; Yang, Z.; Zadjura, L.; Krystal, M.; Meanwell, N. A., Respiratory syncytial virus fusion inhibitors. Part 6: an examination of the effect of structural variation of the benzimidazol-2-one heterocycle moiety. *Bioorg Med Chem Lett* **2007**, *17* (17), 4784-90.
30. Sin, N.; Venables, B. L.; Combrink, K. D.; Gulgeze, H. B.; Yu, K. L.; Civiello, R. L.; Thuring, J.; Wang, X. A.; Yang, Z.; Zadjura, L.; Marino, A.; Kadow, K. F.; Cianci, C. W.; Clarke, J.; Genovesi, E. V.; Medina, I.; Lamb, L.; Krystal, M.; Meanwell, N. A., Respiratory syncytial virus fusion inhibitors. Part 7: structure-activity relationships associated with a series of isatin oximes that demonstrate antiviral activity in vivo. *Bioorg Med Chem Lett* **2009**, *19* (16), 4857-62.
31. Clark, M.; Cramer, R. D.; Van Opdenbosch, N., Validation of the general purpose tripos 5.2 force field. *Journal of Computational Chemistry* **1989**, *10* (8), 982-1012.
32. Cho, S. J.; Tropsha, A., Cross-validated R²-guided region selection for comparative molecular field analysis: a simple method to achieve consistent results. *J Med Chem* **1995**, *38* (7), 1060-6.
33. Trott, O.; Olson, A. J., AutoDock Vina: improving the speed and accuracy of docking with a new scoring function, efficient optimization, and multithreading. *J Comput Chem* **2010**, *31* (2), 455-61.
34. Morris, G. M.; Huey, R.; Lindstrom, W.; Sanner, M. F.; Belew, R. K.; Goodsell, D. S.; Olson, A. J., AutoDock4 and AutoDockTools4: Automated docking with selective receptor flexibility. *J Comput Chem* **2009**, *30* (16), 2785-91.
35. Clark, M.; Cramer, R. D., The Probability of Chance Correlation Using Partial Least Squares (PLS). *Quantitative Structure-Activity Relationships* **1993**, *12* (2), 137-145.

36. Case DA, D. T., Cheatham TE III, Simmerling CL, Wang J, Duke RE, Luo R, Walker RC, Zhang W, Merz KM, et al., AMBER 12. **2012**, San Francisco, CA: University of California.
37. Jorgensen, W. L.; Chandrasekhar, J.; Madura, J. D.; Impey, R. W.; Klein, M. L., Comparison of simple potential functions for simulating liquid water. *The Journal of chemical physics* **1983**, *79* (2), 926-935.
38. Wang, J.; Wolf, R. M.; Caldwell, J. W.; Kollman, P. A.; Case, D. A., Development and testing of a general amber force field. *J Comput Chem* **2004**, *25* (9), 1157-74.
39. Jorgensen, W. L.; Chandrasekhar, J.; Madura, J. D.; Impey, R. W.; Klein, M. L., Comparison of simple potential functions for simulating liquid water. *The Journal of Chemical Physics* **1983**, *79* (2), 926.
40. Darden T, Y. D., Pedersen L, Particle mesh Ewald-- An N-log(N) method for Ewald sums in large systems. *The Journal of Chemical Physics* **1993**, *98*.
41. Burden, F. R., A chemically intuitive molecular index based on the eigenvalues of a modified adjacency matrix. *Quantitative Structure - Activity Relationships* **1997**, *16* (4), 309-314.
42. (a) Wang, W.; Ye, W.; Jiang, C.; Luo, R.; Chen, H. F., New force field on modeling intrinsically disordered proteins. *Chemical biology & drug design* **2014**, *84* (3), 253-69; (b) Chen, H. F.; Luo, R., Binding induced folding in p53-MDM2 complex. *J Am Chem Soc* **2007**, *129* (10), 2930-7; (c) Chen, H.-F., Mechanism of Coupled Folding and Binding in the siRNA-PAZ Complex. *Journal of Chemical Theory and Computation* **2008**, *4* (8), 1360-1368.
43. Wang, J. F.; Yan, J. Y.; Wei, D. Q.; Chou, K. C., Binding of CYP2C9 with diverse drugs and its implications for metabolic mechanism. *Med Chem* **2009**, *5* (3), 263-70.
44. Wickham, H., *ggplot2: elegant graphics for data analysis*. Springer: 2009.
45. Fogolari, F.; Brigo, A.; Molinari, H., Protocol for MM/PBSA molecular dynamics simulations of proteins. *Biophys J* **2003**, *85* (1), 159-66.
46. Miller, B. R.; McGee, T. D.; Swails, J. M.; Homeyer, N.; Gohlke, H.; Roitberg, A. E., MMPBSA.py: An Efficient Program for End-State Free Energy Calculations. *Journal of Chemical Theory and Computation* **2012**, *8* (9), 3314-3321.
47. Gallivan, J. P.; Dougherty, D. A., Cation- π interactions in structural biology. *Proceedings of the National Academy of Sciences* **1999**, *96* (17), 9459-9464.
48. Hunter, C. A.; Sanders, J. K. M., The nature of π - π interactions. *Journal of the American Chemical Society* **1990**, *112* (14), 5525-5534.
49. Wheeler, S. E.; Houk, K. N., Substituent effects in the benzene dimer are due to direct interactions of the substituents with the unsubstituted benzene. *J Am Chem Soc* **2008**, *130* (33), 10854-5.
50. Hong, H.; Xie, Q.; Ge, W.; Qian, F.; Fang, H.; Shi, L.; Su, Z.; Perkins, R.; Tong, W., Mold2, molecular descriptors from 2D structures for chemoinformatics and toxicoinformatics. *Journal of chemical information and modeling* **2008**, *48* (7), 1337-1344.
51. Hao, M.; Li, Y.; Wang, Y.; Zhang, S., A classification study of respiratory Syncytial Virus (RSV) inhibitors by variable selection with random forest. *Int J Mol Sci* **2011**, *12* (2), 1259-80.
52. Lovász, L.; Pelikán, J., On the eigenvalues of trees. *Periodica Mathematica Hungarica* **1973**, *3* (1), 175-182.
53. Randić, M.; Wilkins, C. L., Graph theoretical approach to recognition of structural similarity in molecules. *Journal of Chemical Information and Computer Sciences* **1979**, *19* (1), 31-37.
54. Schrödinger, L., New York, NY, Schrödinger Release 2014-3: Maestro, version 9.9. **2014**.

55. Yan, C.; Xiu, Z.; Li, X.; Li, S.; Hao, C.; Teng, H., Comparative molecular dynamics simulations of histone deacetylase-like protein: binding modes and free energy analysis to hydroxamic acid inhibitors. *Proteins* **2008**, *73* (1), 134-49.
56. Hou, T.; Wang, J.; Li, Y.; Wang, W., Assessing the performance of the MM/PBSA and MM/GBSA methods. 1. The accuracy of binding free energy calculations based on molecular dynamics simulations. *J Chem Inf Model* **2011**, *51* (1), 69-82.

Figure legends:

Figure 1. Interaction surface between BMS-433771 and RSVF protein. A: Two-dimensional representation for the interaction between compound BMS-433771 and core domain of RSVF protein, drawn by Maestro⁵⁴ software. B: Surface of binding pocket colored by residue type (green: hydrophobic; cyan: polar; blue: positive; red: negative)

Figure 2. RMSD for BMS-433771 complex and interaction between BMS-433771 and RSVF. A: RMSD for receptor, all atoms of BMS-433771 and heavy atoms in the core of BMS-433771 in simulation for BMS-433771/RSVF complex. B: Interaction between BMS-433771 and RSVF protein.

Figure 3. Average structure of BMS-433771 and RSVF. A: Average structure for last 5ns. B: Superimposition of initial structure and average structure for last 5ns.

Figure 4. RMSDs for complex, ligand, and skeleton of ligand. A: RMSD of receptor for six complexes and apo-RSVF. B: RMSD of ligands. C: RMSD of skeleton for ligands.

Figure 5. Comparison between G1-8 and G1-168. A: Distance between side chain of V192@E and benzene ring at M1. B: Distance between side chain of D194@A and R₂. C: Alignment of average structure for G1-8 (cyan) and G1-168 (orange) within binding pocket of RSVF. D: Decomposition contribution of binding free energy for ligands.

Figure 6. Comparison of positively-charged G2-126 and negatively charged G2-55.

Figure 7. Violin plot of distance and dihedral angle for different complexes. Violin plot shows the distribution of data, which means the more centralized the data is, the flatter the figure is horizontally and vice versa. A: Violin plot of distances for the π - π of M₂ and Y198 in complexes. B: Violin plot of dihedral angles for the π - π of M₂ and Y198 in complexes.

Figure 8. Dot plot for distance between mass center of M₁ and NZ of K196@E *versus* distance between mass center of M₂ and NZ of K196@E. The number represents the average position for corresponding complex.

Figure 9. Correlation between pEC50 and binding free energy.

Figure 10. Superimposition of average structure for G1-8(blue), G2-126(green), and G3-80(orange) complex.

Figure 11. Correlations between experimental and predictive activity for RSVF inhibitors. A: CoMFA model. B: CoMSIA model. G2-317 is outlier for CoMSIA model.

Figure 12. CoMFA Contour plot with G3-80. A: Contour map of steric field in CoMFA. B: Contour map of Electrostatic field in CoMFA. Yellow contours indicate regions where bulky groups are unfavorable for activity and green contours indicate regions where bulky groups are favorable for activity. Red contours indicate regions where groups with negative charge could increase activity whereas blue contours indicate regions where groups with positive charge could increase activity.

Figure 13. Superposition of CoMSIA model and complex for G3-80/RSVF. G3-80 is marked in orange.

Figure 14. Detail guide for how to improve the bioactivity of inhibitor.

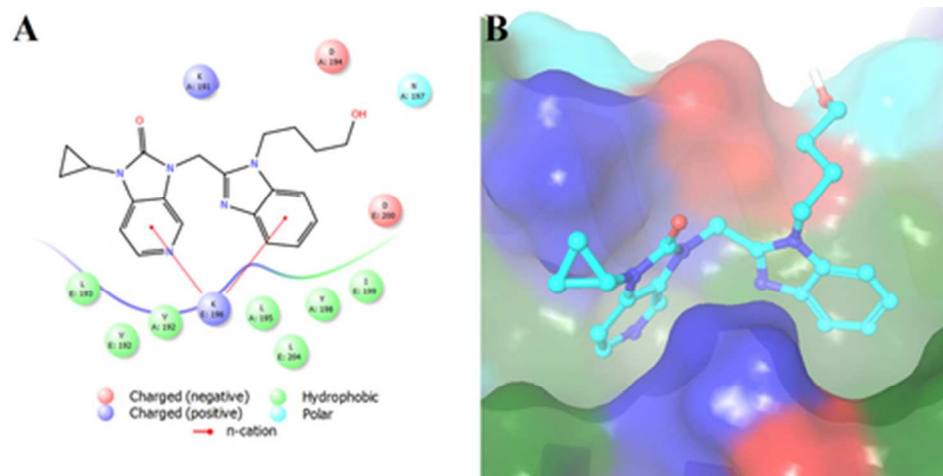
Table 1. Binding free energy with MM/GBSA

Contribution	BMS-433771	G1-8	G1-168	G2-126	G2-55	G3-80	G3-361
VDW	-36.046	-40.282	-39.446	-35.405	-29.032	-33.36	-30.383
EEL	-13.246	-13.767	-6.263	-5.509	-57.296	-3.493	-24.094
EGB	25.394	31.602	27.158	12.833	73.298	12.84	35.877
ΔG_{ele}	12.148	17.835	20.895	7.324	16.002	9.347	11.783
ESURF	-4.391	-5.023	-4.621	-4.723	-3.471	-4.26	-3.897
ΔG_{Gas}	-49.292	-54.049	-45.708	-40.914	-86.328	-36.854	-54.478
ΔG_{Solv}	21.003	26.579	22.537	8.111	69.827	8.579	31.98
ΔG_{Total}	-28.289	-27.471	-23.172	-32.803	-16.501	-28.275	-22.497
pEC50	7.678	8.301	4.975	8.699	3.578	8.523	4.288

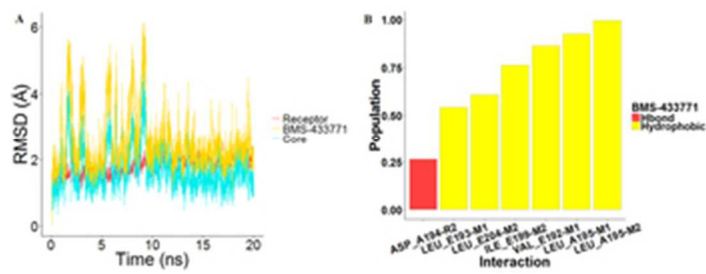
VDW: van der Waals energy; EEL: Electrostatic energy; EGB: Polar solvation energy; ΔG_{ele} : (EEL+EGB) Electrostatic contribution (EEL compensated by EGB^{55,56}); ESURF: Non-polar solvation energy; $\square G_{Gas}$: (VDW+EEL) gas-phase free energy; $\square G_{Solv}$: (EGB+ESURF) solvation free energy; $\square G_{Total}$: ($G_{Gas}+G_{Solv}$) total free energy.

Table 2. PLS statistics parameter for 3D-QSAR model.

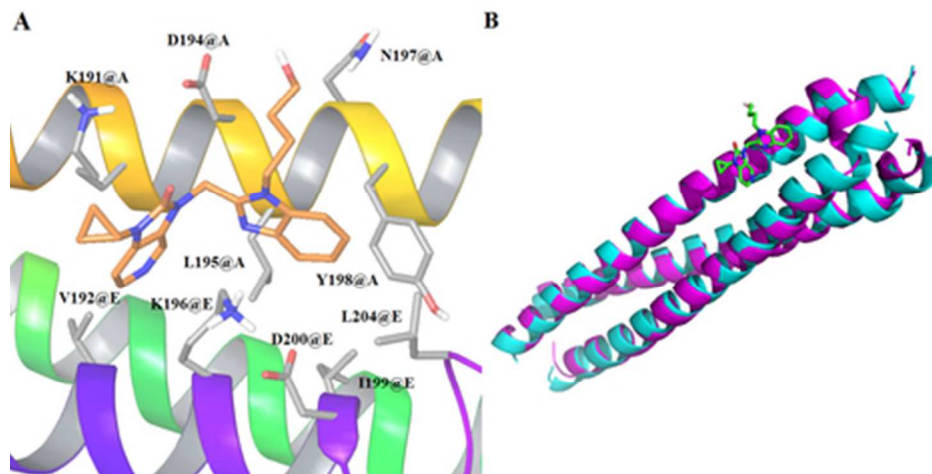
Statistics of QSAR	CoMFA	CoMSIA
Components	11	8
Q^2	0.821	0.795
R^2	0.973	0.961
F	883.058	838.846
SEE	0.188	0.225
RMSE	0.238	0.310
R^2 (test)	0.949	0.914
Hydrophobic	-	0.187
Steric	0.378	0.104
Electrostatic	0.622	0.258
Hydrogen bond Donor	-	0.186
Hydrogen bond Acceptor	-	0.265



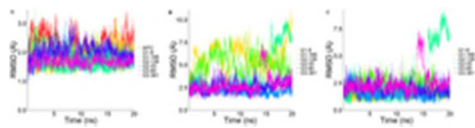
Interaction surface between BMS-433771 and RSVF protein. A: Two-dimensional representation for the interaction between compound BMS-433771 and core domain of RSVF protein, drawn by Maestro54 software. B: Surface of binding pocket colored by residue type (green: hydrophobic; cyan: polar; blue: positive; red: negative)
39x19mm (300 x 300 DPI)



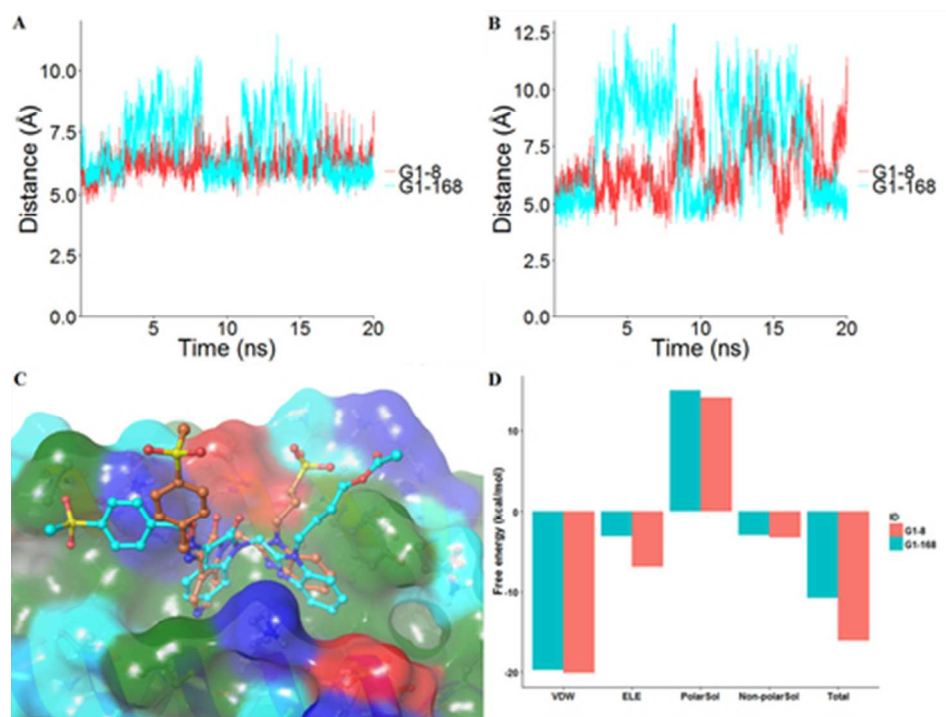
RMSD for BMS-433771 complex and interaction between BMS-433771 and RSVF. A: RMSD for receptor, all atoms of BMS-433771 and heavy atoms in the core of BMS-433771 in simulation for BMS-433771/RSVF complex. B: Interaction between BMS-433771 and RSVF protein.
29x11mm (300 x 300 DPI)



Average structure of BMS-433771 and RSVF. A: Average structure for last 5ns. B: Superimposition of initial structure and average structure for last 5ns.
39x19mm (300 x 300 DPI)

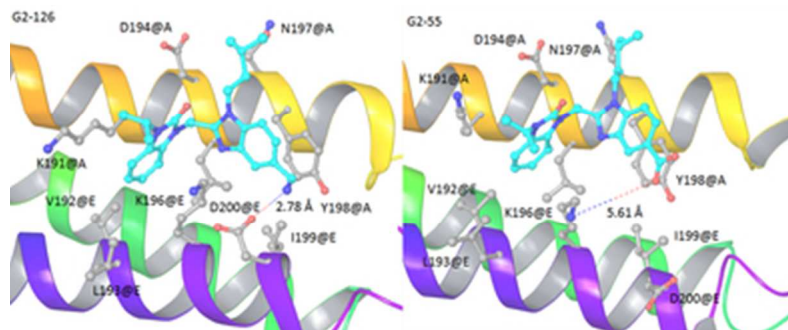


RMSDs for complex, ligand, and skeleton of ligand. A: RMSD of receptor for six complexes and apo-RSVF. B: RMSD of ligands. C: RMSD of skeleton for ligands.
19x4mm (300 x 300 DPI)

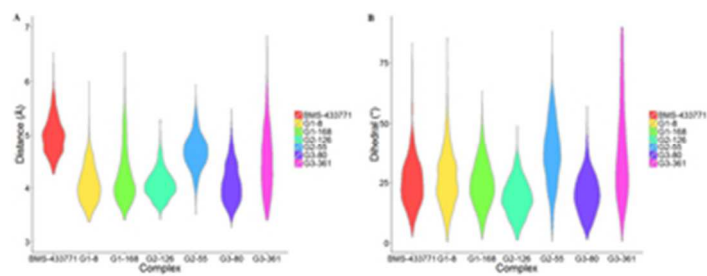


Comparison between G1-8 and G1-168. A: Distance between side chain of V192@E and benzene ring at M1. B: Distance between side chain of D194@A and R2. C: Alignment of average structure for G1-8 (cyan) and G1-168 (orange) within binding pocket of RSVF. D: Decomposition contribution of binding free energy for ligands.

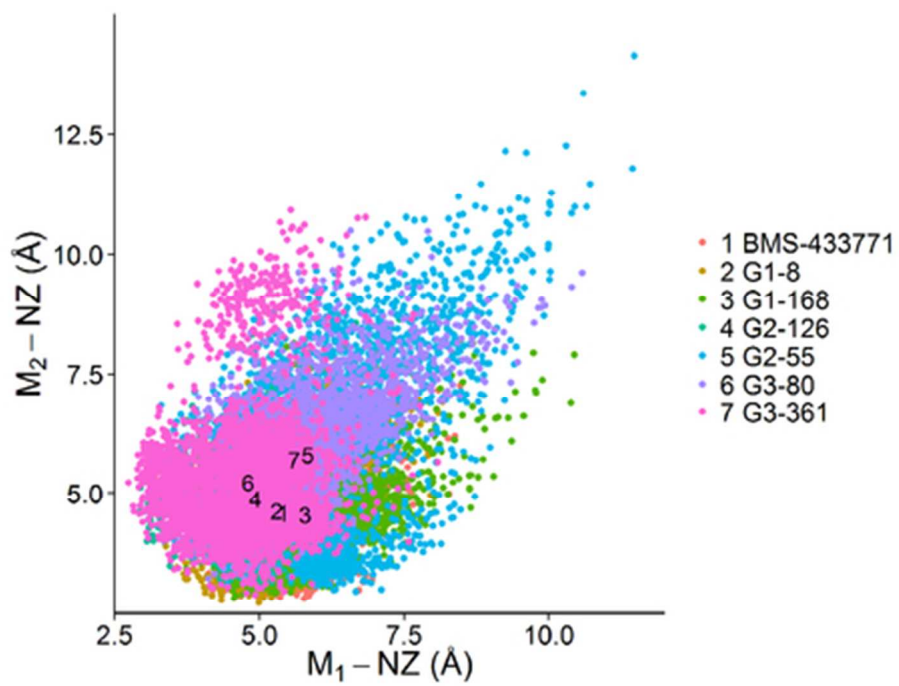
40x30mm (300 x 300 DPI)



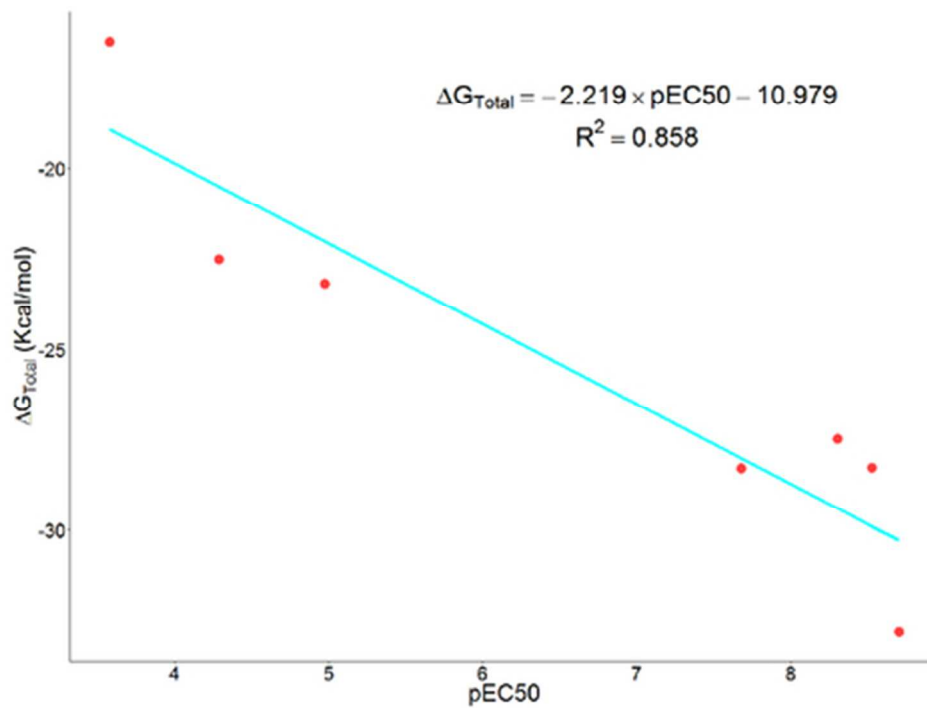
Comparison of positively-charged G2-126 and negatively charged G2-55.
33x13mm (300 x 300 DPI)



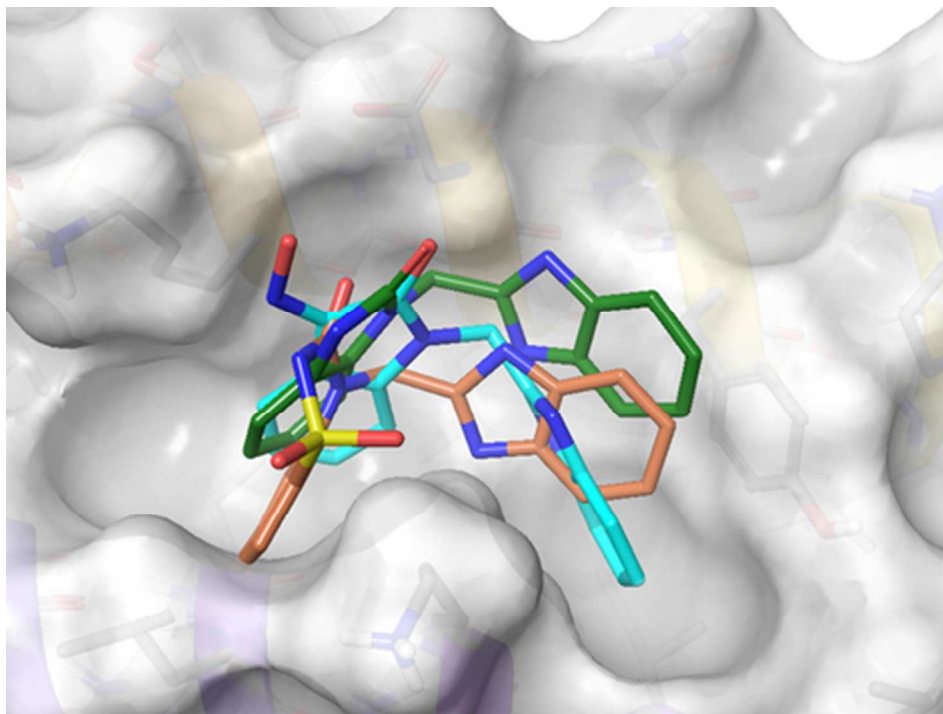
Violin plot of distance and dihedral angle for different complexes. Violin plot shows the distribution of data, which means the more centralized the data is, the flatter the figure is horizontally and vice versa. A: Violin plot of distances for the pi-pi of M2 and Y198 in complexes. B: Violin plot of dihedral angles for the pi-pi of M2 and Y198 in complexes.
29x11mm (300 x 300 DPI)



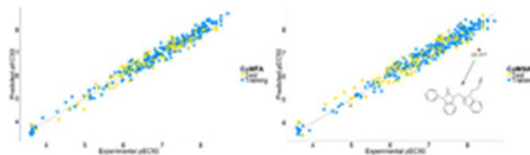
Dot plot for distance between mass center of M1 and NZ of K196@E versus distance between mass center of M2 and NZ of K196@E. The number represents the average position for corresponding complex.
39x29mm (300 x 300 DPI)



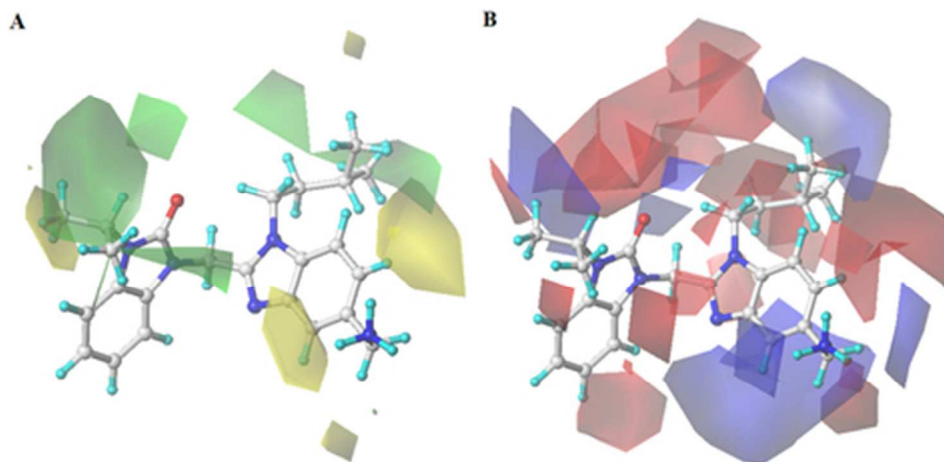
Correlation between pEC50 and binding free energy.
39x29mm (300 x 300 DPI)



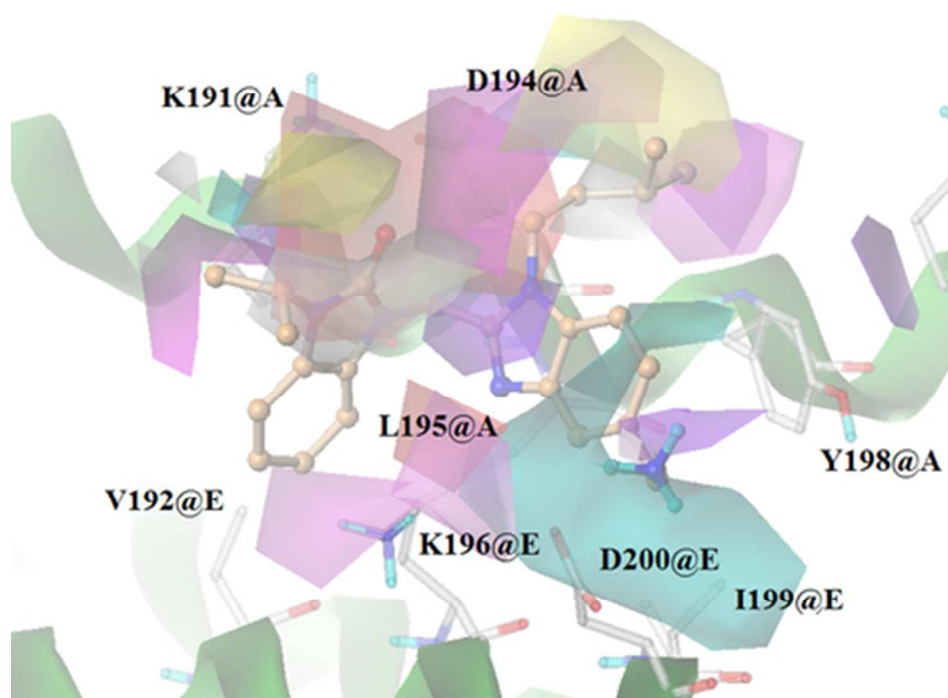
Superimposition of average structure for G1-8(blue), G2-126(green), and G3-80(orange) complex.
39x29mm (300 x 300 DPI)



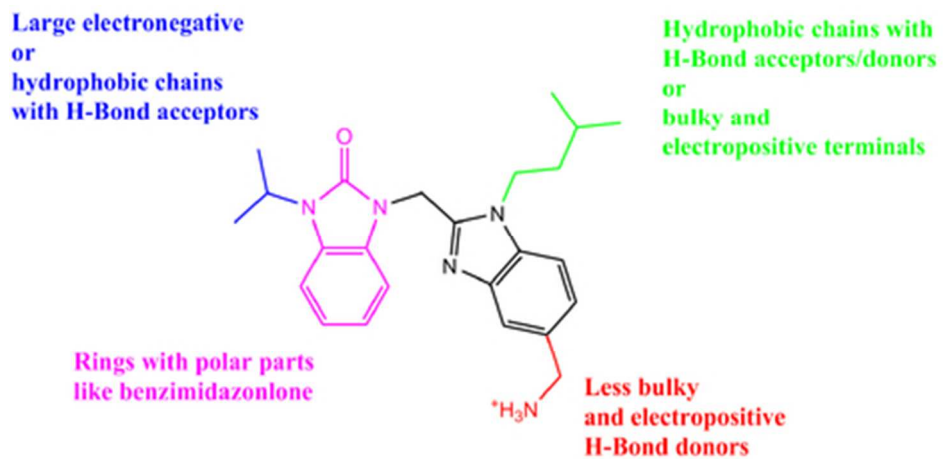
Correlations between experimental and predictive activity for RSVF inhibitors. A: CoMFA model. B: CoMSIA model. G2-317 is outlier for CoMSIA model.
22x6mm (300 x 300 DPI)



CoMFA Contour plot with G3-80. A: Contour map of steric field in CoMFA. B: Contour map of Electrostatic field in CoMFA. Yellow contours indicate regions where bulky groups are unfavorable for activity and green contours indicate regions where bulky groups are favorable for activity. Red contours indicate regions where groups with negative charge could increase activity whereas blue contours indicate regions where groups with positive charge could increase activity.
39x19mm (300 x 300 DPI)



Superposition of CoMSIA model and complex for G3-80/RSVF. G3-80 is marked in orange.
39x29mm (300 x 300 DPI)



Detail guide for how to improve the bioactivity of inhibitor.
39x19mm (300 x 300 DPI)